



CHORUS

This is the accepted manuscript made available via CHORUS. The article has been published as:

Superdeformed and Triaxial States in ^{42}Ca

K. Hadyńska-Klęk *et al.*

Phys. Rev. Lett. **117**, 062501 — Published 1 August 2016

DOI: [10.1103/PhysRevLett.117.062501](https://doi.org/10.1103/PhysRevLett.117.062501)

Superdeformed and triaxial states in ^{42}Ca

K. Hadyńska-Kleń, ^{1,2,3,4} P.J. Napiorkowski, ¹ M. Zielińska, ^{5,1} J. Srebrny, ¹ A. Maj, ⁶ F. Azaiez, ⁷
J.J. Valiente Dobón, ⁴ M. Kicińska-Habior, ² F. Nowacki, ⁸ H. Naïdja, ^{8,9,10} B. Bounthong, ⁸ T. R. Rodríguez, ¹¹
G. de Angelis, ⁴ T. Abraham, ¹ G. Anil Kumar, ⁶ D. Bazzacco, ^{12,13} M. Bellato, ¹² D. Bortolato, ¹² P. Bednarczyk, ⁶
G. Benzoni, ¹⁴ L. Berti, ⁴ B. Birkenbach, ¹⁵ B. Bruyneel, ¹⁵ S. Brambilla, ¹⁴ F. Camera, ^{14,16} J. Chavas, ⁵
B. Cederwall, ¹⁷ L. Charles, ⁸ M. Ciemała, ⁶ P. Cocconi, ⁴ P. Coleman-Smith, ¹⁸ A. Colombo, ¹² A. Corsi, ^{14,16}
F.C.L. Crespi, ^{14,16} D.M. Cullen, ¹⁹ A. Czermak, ⁶ P. Désesquelles, ^{20,21} D.T. Doherty, ^{5,22} B. Dulny, ⁶ J. Eberth, ¹⁵
E. Farnea, ^{12,13} B. Fornal, ⁶ S. Franchoo, ⁷ A. Gadea, ²³ A. Giaz, ^{14,16} A. Gottardo, ⁴ X. Grave, ⁷ J. Grębosz, ⁶
A. Görge, ³ M. Gulmini, ⁴ T. Habermann, ⁹ H. Hess, ¹⁵ R. Isocrate, ^{12,13} J. Iwanicki, ¹ G. Jaworski, ¹ D.S. Judson, ²⁴
A. Jungclaus, ²⁵ N. Karkour, ²¹ M. Kmiecik, ⁶ D. Karpiński, ² M. Kisieliński, ¹ N. Kondratyev, ²⁶ A. Korichi, ²¹
M. Komorowska, ^{1,2} M. Kowalczyk, ¹ W. Korten, ⁵ M. Krzysiek, ⁶ G. Lehaut, ²⁷ S. Leoni, ^{14,16} J. Ljungvall, ²¹
A. Lopez-Martens, ²¹ S. Lunardi, ^{12,13} G. Maron, ⁴ K. Mazurek, ⁶ R. Menegazzo, ^{12,13} D. Mengoni, ¹² E. Merchán, ^{9,28}
W. Męczyński, ⁶ C. Michelagnoli, ^{12,13} J. Mierzejewski, ¹ B. Million, ¹⁴ S. Myalski, ⁶ D.R. Napoli, ⁴ R. Nicolini, ¹⁴
M. Niikura, ⁷ A. Obertelli, ⁵ S.F. Özmen, ¹ M. Palacz, ¹ L. Próchniak, ¹ A. Pullia, ^{14,16} B. Quintana, ²⁹ G. Rampazzo, ⁴
F. Recchia, ^{12,13} N. Redon, ²⁷ P. Reiter, ¹⁵ D. Rosso, ⁴ K. Rusek, ¹ E. Sahin, ⁴ M.-D. Salsac, ⁵ P.-A. Söderström, ³⁰
I. Stefan, ⁷ O. Stężowski, ²⁷ J. Styczeń, ⁶ Ch. Theisen, ⁵ N. Toniolo, ⁴ C.A. Ur, ^{12,13} V. Vandone, ^{14,16}
R. Wadsworth, ²² B. Wasilewska, ⁶ A. Wiens, ¹⁵ J.L. Wood, ³¹ K. Wrzosek-Lipska, ¹ and M. Ziębliński ⁶

¹Heavy Ion Laboratory, University of Warsaw, Pasteura 5A, PL 02-093 Warsaw, Poland

²Faculty of Physics, University of Warsaw, PL 00-681 Warsaw, Poland

³Department of Physics, University of Oslo, N-0316 Oslo, Norway

⁴INFN Laboratori Nazionali di Legnaro, Viale dell'Università, 2, I-35020 Legnaro, Italy

⁵CEA Saclay, IRFU/SPhN, F-91191 Gif-sur-Yvette, France

⁶Institute of Nuclear Physics, Polish Academy of Sciences, PL 31-342 Kraków, Poland

⁷Institut de Physique Nucléaire d'Orsay, F-91400 Orsay, France

⁸Université de Strasbourg, IPHC/CNRS, UMR7178, 23 rue du Loess, F-67037 Strasbourg, France

⁹GSI Helmholtzzentrum für Schwerionenforschung GmbH, D-64291 Darmstadt, Germany

¹⁰LPMS, Université Constantine 1, Route Ain-El bey, 25000 Constantine, Algérie

¹¹Universidad Autónoma de Madrid, Departamento de Física Teórica, Madrid, Spain

¹²INFN Sezione di Padova, I-35131 Padova, Italy

¹³Dipartimento di Fisica e Astronomia dell'Università degli Studi di Padova, I-35131 Padova, Italy

¹⁴Dipartimento di Fisica dell'Università degli Studi di Milano, I-20133 Milano, Italy

¹⁵Institut für Kernphysik, Universität zu Köln, Zùlpicher Straße 77, D-50937 Köln, Germany

¹⁶INFN Sezione di Milano, I-20133 Milano, Italy

¹⁷Department of Physics, Royal Institute of Technology, SE-10691 Stockholm, Sweden

¹⁸Daresbury Laboratory, Daresbury, Warrington WA4 4AD, UK

¹⁹Schuster Laboratory, School of Physics and Astronomy,
The University of Manchester, Manchester, M13 9PL, UK

²⁰Université Paris-Sud, F-91400 Orsay, France

²¹Centre de Spectrométrie Nucléaire et de Spectrométrie de Masse (CSNSM/IN2P3/CNRS), F-91405 Orsay, France

²²Department of Physics University of York, Heslington, York, YO10 5DD, UK

²³Instituto de Física Corpuscular IFIC, CSIC-University of Valencia, S-46980 Paterna, Valencia, Spain

²⁴Oliver Lodge Laboratory, The University of Liverpool, Liverpool, L69 7ZE, UK

²⁵Instituto de Estructura de la Materia, CSIC, Madrid, E-28006 Madrid, Spain

²⁶Flerov Laboratory of Nuclear Reactions JINR, RU-141980 Dubna, Russia

²⁷Université Lyon 1, CNRS, IN2P3, IPN Lyon, F-69622 Villeurbanne, France

²⁸Technische Universität Darmstadt, D-64289 Darmstadt, Germany

²⁹Laboratorio de Radiaciones Ionizantes, Departamento de Física Fundamental, Universidad de Salamanca, Spain

³⁰Department of Physics and Astronomy, Uppsala University, SE-75120 Uppsala, Sweden

³¹School of Physics, Georgia Institute of Technology, Atlanta, Georgia 30332-0430, USA

(Dated: May 23, 2016)

Shape parameters of a weakly-deformed ground-state band and highly-deformed slightly triaxial side band in ^{42}Ca were determined from E2 matrix elements measured in the first low-energy Coulomb excitation experiment performed with AGATA. The picture of two coexisting structures is well reproduced by new state-of-the-art large-scale shell model and beyond-mean-field calculations. Experimental evidence for superdeformation of the band built on 0_2^+ has been obtained and the role of triaxiality in the $A \sim 40$ mass region is discussed. Furthermore, the potential of Coulomb excitation as a tool to study superdeformation has been demonstrated for the first time.

Highly-deformed nuclear shapes, of elongation that may be approximately represented as an ellipsoid with a 2:1 major to minor axes ratio, were first observed in fission isomers in 1962 [1]. This discovery was followed by the observation of superdeformed (SD) bands in the rare-earth region [2]. A particularity of these structures, which are found to occur at high spin, was that their linking to the ground state band was difficult to establish. The phenomenon of superdeformation became a challenge for both experiment and nuclear structure theory, and soon very similar structures have been found in other mass regions, namely $A \sim 130$ [3, 4] and $A \sim 190$ [5]. However, the original criterion of a 2:1 axes ratio does not seem to be universally valid, as the deformation of most of established SD bands corresponds to axes ratios of between 3:2 and 2:1. Recently, SD bands have been discovered in lighter nuclei, particularly in the $A \sim 40$ mass region, where the nucleons occupy similar proton and neutron orbitals. The deformation parameter, β , in the side bands of ^{40}Ca [6] $^{36,38,40}\text{Ar}$ [7–10] and ^{44}Ti [11] nuclei reaches 0.4 - 0.6, which is similar to what is observed in other mass regions, where superdeformation has been established. However, in contrast to heavier nuclei, strongly deformed bands in $A \sim 40$ isotopes are linked to other, less deformed states by intense γ -ray transitions.

Considering the relatively small number of nucleons, the $A \sim 40$ region constitutes an excellent testing ground to study the origin of highly-deformed structures within various theoretical approaches, such as, for example, large scale shell model (SM) [12, 13], beyond-mean-field models (BMF) [14–16] and antisymmetrized molecular dynamics (AMD) [17–22]. In particular, the normal-deformed (ND) and SD structures in ^{40}Ca were successfully described in the framework of SM calculations that yielded a spherical ground-state band, a ND band ($\beta=0.3$) built on the 0_2^+ state dominated by the $4p - 4h$ excitation into the pf shell, and a SD band ($\beta=0.6$) built on the 0_3^+ state with an $8p - 8h$ configuration [13]. The side band observed in this nucleus at low excitation energy was interpreted as a partner of the $4p - 4h$ excited band, resulting from its triaxial shape, which is in agreement with the conclusions of other theoretical works [18, 23, 24]. The importance of the triaxial degree of freedom in the development of deformation was also suggested for other nuclei in this mass region, e.g. ^{44}Ti [17]. The currently available experimental data, however, are not conclusive, as they are mostly limited to energies of states in gamma bands. More solid evidence for triaxiality can be obtained from a measurement of transition probabilities and quadrupole moments of excited states.

A regular side band built on the 0_2^+ state is known in ^{42}Ca , and some of its spectroscopic properties do not differ significantly from those of the established SD bands in the $A \sim 40$ region. Firstly, its moment of inertia, which is proportional to the quadrupole deformation parameter

β_2 [25], is large and similar to those in the SD bands in ^{36}Ar and ^{40}Ca . The strongly deformed character of this band is further supported by the observation of its preferential feeding from the low-energy component of the highly-split giant dipole resonance decay of ^{46}Ti [26]. On the other hand, the lifetimes of the states in the side band [27, 28] indicate that their deformation is smaller than that of the SD band in ^{40}Ca ; it should be noted, however, that these lifetimes are subject to significant uncertainties.

Since the band head of the side band in ^{42}Ca lies at excitation energy of 1837 keV, considerably lower than its counterparts in the neighboring Ca and Ar isotopes, it is possible to populate this structure by Coulomb excitation in order to obtain a complete set of electromagnetic matrix elements between the observed states. This includes spectroscopic quadrupole moments that are directly related to the charge distribution in a given state, as well as transitional quadrupole matrix elements, which can be used to infer the mixing between the observed structures using comparisons with state-of-the-art model calculations.

In this Letter, we report on the results of a dedicated Coulomb excitation experiment to study properties of the superdeformed band in ^{42}Ca , performed at the Laboratori Nazionali di Legnaro, Italy [29, 30]. A ^{42}Ca beam of 170 MeV energy bombarded 1 mg/cm² thick targets of ^{208}Pb and ^{197}Au . The γ rays from Coulomb excited nuclei were measured with the three triple clusters of AGATA [31] in coincidence with back-scattered projectiles, detected in the DANTE array [32, 33] consisting of three Micro-Channel Plate (MCP) detectors, covering θ_{LAB} angles from 100° to 144° .

Thanks to the combination of two position-sensitive detector arrays, DANTE for charged particles and the AGATA tracking spectrometer for γ rays, the observation and Doppler correction of the γ transitions deexciting the ground state and side bands in ^{42}Ca were possible (see Fig. 1). The γ -ray spectrum obtained with the ^{208}Pb target, Doppler corrected for the ^{42}Ca velocity, in coincidence with back-scattered particles registered in one of the MCP detectors, is shown in Fig. 2. In addition to transitions resulting from Coulomb excitation of ^{42}Ca and ^{208}Pb , weaker lines at 376, 1674 and 2048 keV are observed, originating from the sub-barrier transfer reaction $^{208}\text{Pb}(^{42}\text{Ca}, ^{43}\text{Ca})^{207}\text{Pb}$ (as discussed in [30]). A Doppler-broadened and shifted 511-keV γ -ray line, and transitions from Coulomb excitation of target impurities: ^{204}Pb (899 keV), ^{206}Pb (803 keV), ^{207}Pb (570 keV), are also present in the spectrum. The transition in ^{204}Pb obscured the $2_2^+ \rightarrow 2_1^+$ line in ^{42}Ca , therefore the intensity of the latter could only be extracted from the data collected with the ^{197}Au target (see inset in Fig. 2).

A set of reduced electromagnetic matrix elements between the low-lying states in ^{42}Ca was extracted us-

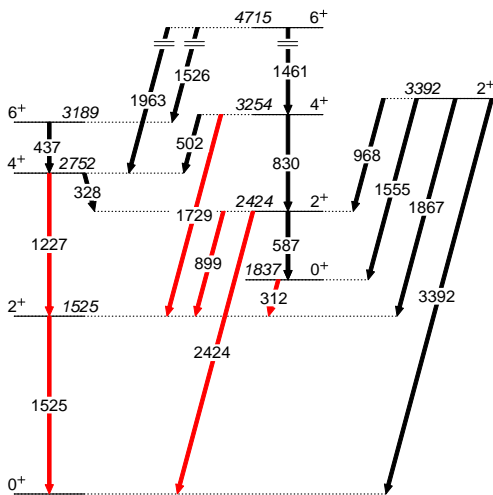


FIG. 1. (Color online) Low-lying excited states in ^{42}Ca , considered in the present analysis [35]. Transitions observed in the current experiment are marked in red. Level and transition energies are given in keV.

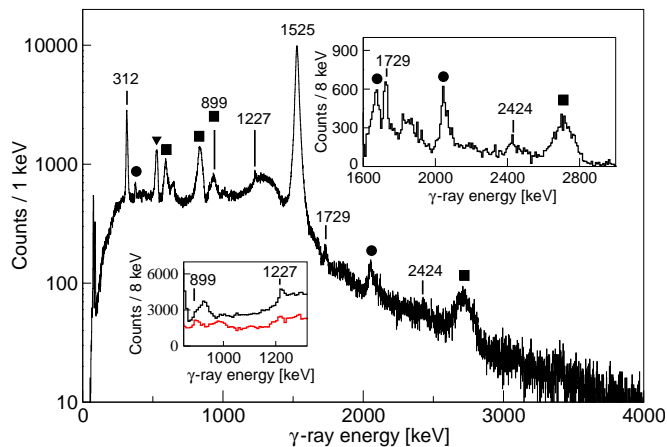


FIG. 2. (Color online) The γ -ray spectrum observed in the $^{42}\text{Ca}+^{208}\text{Pb}$ Coulomb excitation experiment in coincidence with back-scattered particles registered in one of MCP detectors and Doppler corrected for the projectile. The lines not originating from ^{42}Ca are marked as follows: \blacksquare – lead isotopes, \blacktriangledown – 511 keV, \bullet – ^{43}Ca . Insets show portions of the spectrum zoomed on the 1600–3000 keV and 850–1300 keV energy ranges, the latter presenting also the spectrum collected with the ^{197}Au target (in red, multiplied by a factor of 3 for presentation purpose).

ing the GOSIA code [34]. It was fitted to the observed γ -ray yields, as well as to the known spectroscopic data for ^{42}Ca : lifetimes of the yrast and non-yrast states [27, 36–45], E2/M1 mixing ratios [28, 47], the quadrupole moment of the 2_1^+ state [36], and the branching ratios [45, 46, 48, 49]. In particular, the $2_2^+ \rightarrow 0_1^+/2_2^+ \rightarrow 2_1^+$ branching ratio was remeasured at the Heavy Ion Laboratory, University of Warsaw, Poland, using the $^{12}\text{C}(^{32}\text{S}, 2p)^{42}\text{Ca}$ fusion-evaporation reaction,

employing the EAGLE Compton-suppressed HPGe detector array [50]. The obtained value, 0.35(7), which is in agreement with the previous findings [45], was used to constrain the Coulomb excitation data analysis. Although no transitions de-exciting the 2_3^+ state were observed in the present experiment, its influence on the population of other states was taken into account by introducing into the calculations matrix elements coupling it to the observed states. These were calculated from the known spectroscopic data, such as the lifetime of the 2_3^+ state and branching and mixing ratios for all possible paths of its decay [35], and remained fixed in the GOSIA minimization routine.

It should also be noted that although the $2_2^+ \rightarrow 0_2^+$ transition is too weak to be observed, the corresponding matrix element affects excitation cross sections of observed states, in particular that of the 2_2^+ , and hence it could be determined from the intensities measured in the present Coulomb excitation experiment.

The resulting set of reduced matrix elements in ^{42}Ca and corresponding $B(E2)$ values are presented in Table I. Two key pieces of information regarding the deformation of the side band have been obtained for the first time: the $\langle 2_2^+ || E2 || 0_2^+ \rangle$ matrix element, as well as the spectroscopic quadrupole moment of the 2_2^+ state. Their values are consistent with a large quadrupole deformation of this band. Other matrix elements obtained in the present analysis are in general agreement with the results of earlier measurements, and in several cases the precision has been considerably improved, notably for transitions de-exciting the 4_2^+ state.

In order to get a complete picture of the coexisting structures in ^{42}Ca , two new SM and BMF calculations have been performed.

Following the previous description [13] of the spherical, normal-deformed and superdeformed structures in ^{40}Ca , SM calculations have been carried out using up to 6 particle-hole excitations from the $s_{1/2}$ and $d_{3/2}$ orbitals into the pf orbitals. This is computationally challenging, with matrices of dimensions $O(10^9)$, and was tackled using the m -scheme code ANTOINE [51, 52]. The effective charges used were $1.5e$ for protons and $0.5e$ for neutrons. The results show that the configuration of the 0_2^+ and 2_2^+ states is dominated by the $6p - 4h$ excitation, which is supported by the α transfer strength to the 0_2^+ state in ^{42}Ca measured with the $^{38}\text{Ar}(^6\text{Li}, d)^{42}\text{Ca}$ reaction [53]. The above results are in agreement with the earlier deformed-basis AMD+GCM model calculations [54] that predicted $\beta=0.43$ for the band built on the 0_2^+ state of $6p - 4h$ configuration. Furthermore, the importance of triaxiality in this system has been clearly revealed: the spectroscopic quadrupole moment of the 2_3^+ state has been found to be of similar magnitude ($19 e \text{ fm}^2$) but of opposite sign to that of the 2_2^+ state. In addition, the calculations yielded a low-lying 3^+ state, which is connected by a strong transition to the 2_3^+ state ($B(E2; 3^+ \rightarrow$

2_3^+)= $372 e^2 fm^4$) and has a spectroscopic quadrupole moment close to zero. Hence, these states were identified as members of the SD gamma band built on the 2_3^+ level, having a structure dominated by the $6p - 4h$, similar to that of the 2_2^+ and 0_2^+ states. Constrained Hartree-Fock calculations (CHFSM) performed with the same Hamiltonian and within the same valence space [55] presented in Fig. 3 (left), revealed a first triaxial minimum at $\beta=0.4$ and with γ close to 20° , and a second minimum at $\beta = 0.6$ and $\gamma = 8^\circ$. In contrast, the ground state band is based on a spherical minimum, dominated by a two-particle configuration, but with a considerable amount of $4p - 2h$ and $6p - 4h$ admixtures.

In the BMF calculations, particle number and angular momentum symmetry restorations have been taken into account as well as quadrupole (axial and non-axial) shape mixing within a generator coordinate method. The Gogny D1S interaction was used to define the corresponding energy density functional [56]. These calculations yielded a similar general picture of a spherical ground-state band, a deformed triaxial rotational band built on top of the 0_2^+ state, and a gamma band associated to it.

Matrix elements calculated using these two approaches are presented in Table I. The general picture of two co-existing structures differing in collectivity is well reproduced. However, both theoretical predictions overestimate in-band matrix elements in the side band, and underestimate the corresponding spectroscopic quadrupole moments, which suggests that this structure may be more axially symmetric and slightly less deformed than that predicted by theory. On the other hand, quadrupole moments and transition probabilities in the ground-state band are underestimated by both models, as well as intra-band transition rates, which means that the mixing between the two bands is not fully reproduced.

Comparisons of individual matrix elements may not always be conclusive, thus the obtained E2 matrix elements, both experimental and theoretical, were further interpreted in the framework of the quadrupole sum method [57–59] in order to extract information on the charge distribution of the nucleus in specific states. In this method, which has been recently applied to $^{182-188}\text{Hg}$ [60] and $^{96,98}\text{Sr}$ [61], the quadrupole rotational invariants, $\langle Q^2 \rangle$ and $\langle Q^3 \cos(3\delta) \rangle$, are calculated from experimentally determined matrix elements. The first of them is a measure of overall deformation and is proportional to the sum of squared E2 matrix elements $\langle i || E2 || t \rangle \langle t || E2 || i \rangle$ over all intermediate states $|t\rangle$ that can be reached from the state in question $|i\rangle$ in a single E2 transition. The higher-order invariant $\langle Q^3 \cos(3\delta) \rangle$ that provides information on axial symmetry, is constructed of triple products of E2 matrix elements ($\langle i || E2 || t \rangle \langle t || E2 || u \rangle \langle u || E2 || i \rangle$, where $|i\rangle$ – initial state, $|t\rangle$ and $|u\rangle$ – intermediate states) and thus relative signs of E2 matrix elements entering the sum must

TABLE I. Reduced transitional and diagonal E2 matrix elements between the low-lying states in ^{42}Ca and corresponding $B(E2)$ values and spectroscopic quadrupole moments. Present experimental results are compared with previously measured values, SM and BMF calculations.

$I_i^+ \rightarrow I_f^+$	$\langle I_i E2 I_f \rangle$ [$e \cdot fm^2$]			$B(E2; I_i^+ \rightarrow I_f^+)$ [W.u.]	
	Present	SM	BMF	Present	Previous
$2_1^+ \rightarrow 0_1^+$	$20.5^{+0.6}_{-0.6}$	11.5	9.14	$9.7^{+0.6}_{-0.6}$	9.3 ± 1 [36] 11 ± 2 [28] 9 ± 3 [27] 8.5 ± 1.9 [45]
$4_1^+ \rightarrow 2_1^+$	$24.3^{+1.2}_{-1.2}$	11.3	12.2	$7.6^{+0.7}_{-0.7}$	50 ± 15 [28] 11 ± 3 [27] 10^{+10}_{-8} [45]
$6_1^+ \rightarrow 4_1^+$	$9.3^{+0.2}_{-0.2}$	8.2	14.3	$0.77^{+0.03}_{-0.03}$	0.7 ± 0.3 [27]
$0_2^+ \rightarrow 2_1^+$	$22.2^{+1.1}_{-1.1}$	11.9	6.1	57^{+6}_{-6}	64 ± 4 [27] 100 ± 6 [28] 55 ± 1 [42] 64 ± 4 [45]
$2_2^+ \rightarrow 0_1^+$	$-6.4^{+0.3}_{-0.3}$	9.4	4.4	$1.0^{+0.1}_{-0.1}$	2.2 ± 0.6 [28] 1.5 ± 0.5 [27] 1.2 ± 0.3 [45]
$2_2^+ \rightarrow 2_1^+$	$-23.7^{+2.3}_{-2.7}$	-13.6	-7.7	$12.9^{+2.5}_{-2.5}$	17 ± 11 [28] 19^{+22}_{-14} [27] 14^{+35}_{-9} [45]
$4_2^+ \rightarrow 2_1^+$	42^{+3}_{-4}	21.9	10.1	23^{+3}_{-4}	30 ± 11 [28] 16 ± 5 [27] 12^{+7}_{-4} [45]
$2_2^+ \rightarrow 0_2^+$	26^{+5}_{-3}	32	42	15^{+6}_{-4}	<61 [27] <46 [45]
$4_2^+ \rightarrow 2_2^+$	46^{+3}_{-6}	52	70	27^{+4}_{-6}	60 ± 30 [27] 60 ± 20 [28] 40^{+40}_{-30} [45]
	$\langle I_i E2 I_f \rangle$ [$e \cdot fm^2$]			Q_{sp} [$e \cdot fm^2$]	
$2_1^+ \rightarrow 2_1^+$	-16^{+9}_{-3}	-4.3	0.1	-12^{+7}_{-2}	-19 ± 8 [36]
$2_2^+ \rightarrow 2_2^+$	-55^{+15}_{-15}	-31	-42	-42^{+12}_{-12}	

be known.

The $\langle Q^2 \rangle$ parameters were obtained for the 0^+ and 2^+ states in both bands, as presented in Table II. Since the present measurement yielded relative signs of E2 matrix elements coupling the 0^+ and 2^+ states, it was also possible to determine the $\langle Q^3 \cos(3\delta) \rangle$ invariants for the 0_1^+ and 0_2^+ states (Table II). This is the first time that this kind of information has been obtained in the A ~ 40 mass region.

The same procedure was applied to matrix elements resulting from theoretical calculations. In this case one can include in the calculations all intermediate states obtained from the theory, or just the same subset of states that were used to calculate experimental values of $\langle Q^2 \rangle$

TABLE II. Experimental and theoretical shape parameters $\langle Q^2 \rangle$ [$e^2 \text{fm}^4$], $\sigma(Q^2)$ [$e^2 \text{fm}^4$] and $\langle \cos(3\delta) \rangle$, calculated from $\langle Q^3 \cos(3\delta) \rangle$ as in Ref. [60, 62].

state	$\langle Q^2 \rangle_{exp}$	$\langle Q^2 \rangle_{SM}$	$\sigma(Q^2)_{SM}$	$\langle Q^2 \rangle_{BMF}$	$\sigma(Q^2)_{BMF}$
0_1^+	500 (20)	240	470	100	250
2_1^+	900 (100)	250	490	100	310
0_2^+	1300 (230)	1200	500	1900	520
2_2^+	1400 (250)	1130	500	1900	300

state	$\langle \cos(3\delta) \rangle_{exp}$	$\langle \cos(3\delta) \rangle_{SM}$	$\langle \cos(3\delta) \rangle_{BMF}$
0_1^+	0.06 (10)	0.34	0.34
0_2^+	0.79 (13)	0.67	0.49

and $\langle Q^3 \cos(3\delta) \rangle$. The difference between the results of these two approaches is negligible for all studied states in ^{42}Ca .

A simplistic interpretation of the obtained shape parameters would be that a highly-deformed, non-axial side band coexists with the ground-state band, that is less deformed and maximally triaxial. However, ^{42}Ca , lying only 2 neutrons above the closed $N=20$ shell, is widely considered to be spherical in its ground state, as supported by the potential energy surface maps in Fig. 3. The non-zero $\langle Q^2 \rangle$ value obtained for the 0_1^+ state may thus correspond to fluctuations about a spherical shape. This is consistent with the maximum triaxiality obtained for this state, which in this case would result from averaging over all possible quadrupole shapes. If this interpretation is correct, the dispersion of $\langle Q^2 \rangle$, defined as $\sigma(Q^2) = \sqrt{\langle Q^4 \rangle - \langle Q^2 \rangle^2}$ [63] should be comparable to $\langle Q^2 \rangle$. The existing set of experimentally determined matrix elements, although large, is not sufficient to obtain the $\langle Q^4 \rangle$ invariant. However, it can be determined from the theoretical values of matrix elements in order to get a better understanding of the experimental results.

The behaviour of $\langle Q^2 \rangle$ and its dispersion is remarkably consistent for both theoretical approaches, as shown in Table II. For the ground-state band, $\sigma(Q^2)_{SM}$ and $\sigma(Q^2)_{BMF}$ values are comparable with $\langle Q^2 \rangle$, as one would expect for fluctuations in a spherical minimum of potential. For the side band, however, the dispersion is much lower than the actual value, which is interpreted as a static deformation. In this case, the $\langle Q^2 \rangle$ and $\langle Q^3 \cos(3\delta) \rangle$ invariants can be further converted to the β and γ collective model deformation parameters, as explained in detail in [59].

The $\beta=0.43(2)$ and $\gamma=13(-5)^\circ$ deformation parameters obtained in this way for 0_2^+ , show that the side band in ^{42}Ca has a slightly triaxial superdeformed shape, and can be directly compared to model predictions. A very good overall agreement is found: both potential energy surface maps presented in Fig. 3, in addition to a spherical minimum for the ground-state band show a triaxial minimum that is located at $\beta_2=0.4$ and $\gamma \approx 20^\circ$ for CHFSM (panel

(a)) and at $\beta_2=0.5$, $\gamma = 15^\circ$ for BMF calculations (panel (b)).

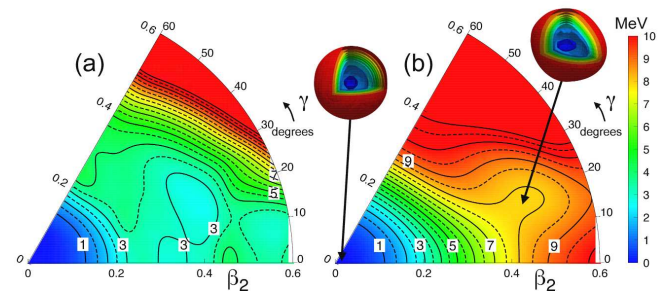


FIG. 3. (Color online) Potential energy surfaces resulting from deformation-constrained Hartree-Fock calculations with (a) SM interaction, and (b) BMF, particle number projection method (PN-VAP), Gogny D1S interaction. Spatial densities corresponding to each minimum found in BMF calculations are also shown in the panel (b).

It should be noted that the deformation predicted by both theoretical approaches remains constant within each band. This is confirmed by the experimental results for the highly-deformed structure, but those for the ground-state band show that the $\langle Q^2 \rangle$ for the 2_1^+ state is considerably larger than the value obtained for the ground state. This effect can be attributed to a possible mixing of the 2^+ states, consistent with one-neutron transfer reaction spectroscopy [64, 65] and the measured intra-band transition strengths that are underestimated by both calculations.

In conclusion, the properties of low-lying states in ^{42}Ca were studied via the measurement of E2 matrix elements using low-energy Coulomb excitation. The quadrupole deformation parameters of the ground state and the side bands in ^{42}Ca were determined from the measured reduced matrix elements and compared with the results of SM and BMF calculations. The non-zero value of the overall deformation parameter $\langle Q^2 \rangle$ for the ground state in ^{42}Ca has been attributed to the fluctuations around the spherical shape. In contrast, a large static deformation of $\beta=0.43(2)$ and $\beta=0.45(2)$, respectively, was observed for the two lowest states in the side band, proving its superdeformed character, therefore, for the first time, the deformation of a SD band was studied using the Coulomb excitation technique. The triaxiality parameter $\langle \cos(3\delta) \rangle$ measured for the 0_2^+ state provides the first experimental evidence for non-axial character of SD bands in the $A \sim 40$ mass region. Both SM and BMF calculations well reproduce the general picture of coexistence of a spherical ground-state band with a slightly triaxial SD band. The correct description of the observed mixing between the two coexisting structures remains a challenge for future theoretical works.

The authors would like to thank Jacek Dobaczewski for the fruitful discussions. We also would like to thank

the members of AGATA and EAGLE collaborations for their hard work for the project. Special gratitude goes to the INFN LNL and HIL Warsaw technical staff, for their support and help, in particular the accelerator crews for providing intense and good-quality ^{42}Ca and ^{32}S beams. K.H.-K. acknowledges support from the Research Council of Norway under the project Grant No. 213442. T.R.R. acknowledges computing time at GSI-Darmstadt and support from Spanish MINECO under Programa Ramon y Cajal 11420 and FIS-2014-53434-P (TRR), H.N. acknowledges support from Helmholtz Association through the Nuclear Astrophysics Virtual Institute NAVI (N $^{\circ}$. VH-VI-417). We also acknowledge the support by Generalitat Valenciana, Spain, under the grant PROMETEOII/2014/019 and by the FEDER funds of the European Commission (A. Gadea), Spanish Ministerio de Economía y Competitividad under contract FPA2014-57196-C5 (A. Jungclauss, A. Gadea), German Bundesministerium für Bildung und Forschung (BMBF) under Contract No. 05P12PKFNE TP4 (B. Birkenbach), the Polish National Science Centre under projects No: DEC-2013/10/M/ST2/00427, DPN/N190/AGATA/2009, 2011/03/B/ST2/01894, UMO-2014/14/M/ST2/00738 (COPIN-INFN Collaboration), 2015/17/B/ST2/01534.

-
- [1] S.M. Polikhanov *et al.*, *Sov. Phys. JETP* **15**, 1016 (1962).
 [2] P.J. Twin *et al.*, *Phys. Rev. Lett.* **57**, 811 (1986).
 [3] P.J. Nolan *et al.*, *J. Phys.* **G 11**, L17 (1985).
 [4] E. M. Beck *et al.*, *Phys. Rev. Lett.* **5**, 2182 (1987).
 [5] E.F. Moore *et al.*, *Phys. Rev. Lett.* **63**, 360 (1989).
 [6] E. Ideguchi *et al.*, *Phys. Rev. Lett.* **87**, 222501 (2001).
 [7] C.E. Svensson *et al.*, *Phys. Rev. Lett.* **85**, 2693 (2000).
 [8] C.E. Svensson *et al.*, *Phys. Rev.* **C63**, 061301 (R) (2001).
 [9] D. Rudolph *et al.*, *Phys. Rev.* **C65**, 034305 (2002).
 [10] E. Ideguchi *et al.*, *Phys. Lett.* **B686**, 18 (2010).
 [11] D.C. O’Leary *et al.*, *Phys. Rev.* **C61**, 064314 (2000).
 [12] E. Caurier, F. Nowacki, and A. Poves, *Phys. Rev. Lett.* **95**, 042502 (2005).
 [13] E. Caurier, J. Menendez, F. Nowacki, and A. Poves, *Phys. Rev.* **C75**, 054317 (2007).
 [14] T. Inakura, S. Mizutori, M. Yamagami, and K. Matsuyanagi, *Nucl. Phys.* **A710**, 261 (2002).
 [15] R.R. Rodriguez-Guzman, J.L. Egido, and L.M. Robledo, *Int. J. Mod. Phys.* **E13**, 139 (2004).
 [16] M. Bender, H. Flocard, and P.H. Heenen, *Phys. Rev.* **C68**, 044321 (2003).
 [17] M. Kimura and H. Horiuchi, *Nucl. Phys.* **767**, 58 (2006).
 [18] Y. Taniguchi, M. Kimura, Y. Kanada-Enyo, and H. Horiuchi, *Phys. Rev.* **C76**, 044317 (2007).
 [19] M. Kimura and H. Horiuchi, *Phys. Rev.* **C69**, 051304 (2004).
 [20] Y. Kanada-Enyo and M. Kimura, *Phys. Rev.* **C72**, 064322 (2005).
 [21] Y. Taniguchi, Y. Kanada-Enyo, and M. Kimura, *Prog. Theor. Phys.* **121**, 533 (2009).
 [22] Y. Taniguchi, Y. Kanada-Enyo, and M. Kimura, *Phys. Rev.* **C80**, 044316 (2009).
 [23] W.J. Gerace and A.M. Green, *Nucl. Phys.* **123**, 241 (1969).
 [24] W.J. Gerace and J.P. Mestre, *Nucl. Phys.* **285**, 253 (1977).
 [25] M. Lach *et al.*, *Eur. Phys. J.* **A16**, 309 (2003).
 [26] M. Kmiecik *et al.*, *Acta Phys. Pol.* **B36**, 1169 (2005).
 [27] R. Hartmann and H. Grawe, *Nucl. Phys.* **164**, 209, (1971).
 [28] N. Lawley *et al.*, *Nucl. Phys.* **159**, 385, (1970).
 [29] K. Hadyńska-Klęk *et al.*, *Acta Phys. Pol.* **B42**, 817 (2011).
 [30] K. Hadyńska-Klęk *et al.*, *Acta Phys. Pol.* **B44**, 617 (2013).
 [31] S. Akkoyun *et al.*, *Nucl. Instr. and Meth.* **A668**, 26 (2012).
 [32] A. Gadea *et al.*, *Nucl. Instr. and Meth.* **A654**, 88 (2011).
 [33] J.J. Valiente-Dobón *et al.*, *Acta Phys. Pol.* **B37**, 225, (2006).
 [34] T. Czosnyka, D. Cline, and C.Y. Wu, *Bull. Am. Phys. Soc.* **28**, 745 (1982), www.slac.stanford.edu/gosia
 [35] Balraj Singh and John A. Cameron *Nuclear Data Sheets* **92**, 1 (2001).
 [36] C.W. Towsley, D. Cline, and R.N. Horoshko, *Nucl. Phys.* **A204**, 574, (1973).
 [37] A.R. Poletti *et al.*, *Phys. Rev.* **C10**, 997 (1974).
 [38] K.P. Lieb and M. Uhrmacher, *Zeit. fur Phys.* **267**, 399, (1974).
 [39] M. Marmor *et al.*, *Phys. Rev. Lett.* **25**, 1033, (1970).
 [40] T. Nomura *et al.*, *Phys. Rev. Lett.* **25**, 1342, (1970).
 [41] R.A. Mendelson and R.T. Carpenter, *Phys. Rev.* **181**, 1552, (1969).
 [42] P.M. Lewis *et al.*, *Nucl. Phys.* **A 443**, 210, (1985).
 [43] R. Hartmann *et al.*, *Nucl. Phys.* **123**, 437, (1969).
 [44] P. Betz *et al.*, *Zeit. fur Phys.* **A276**, 295, (1976).
 [45] W.J. Kossler *et al.*, *Phys. Rev.* **177** 1725, (1969).
 [46] P.M. Endt and C. van der Leun, *Nucl. Phys.* **214**, 1625, (1973),
 [47] H.L. Scott *et al.*, *Nucl. Instr. and Meth.* **70**, 320, (1968).
 [48] K. Kawade *et al.*, *Jour. Phys. Soc. Japan* **29**, 43, (1970).
 [49] P.C. Rogers and G.E. Gordon, *Phys. Rev.* **129**, 2653, (1963).
 [50] J. Mierzejewski *et al.*, *Nucl. Instr. and Meth.* **A659**, 84 (2011).
 [51] A. Caurier and F. Nowacki (published in website).
 [52] E. Caurier, G. Martinez-Pinedo, F. Nowacki, A. Poves, and A.P. Zuker, *Rev. Mod. Phys.* **77**, 427 (2005).
 [53] H.T. Fortune *et al.*, *Nucl. Phys.* **294**, 208, (1978).
 [54] Y. Taniguchi, *Prog. Theor. Exp. Phys.* **073D01**, (2014).
 [55] B. Bounthong, PhD Thesis, Université de Strasbourg (in progress).
 [56] T.R. Rodriguez and J.L. Egido, *Phys. Rev.* **C81**, 064323, (2010).
 [57] D. Cline, *Annu. Rev. Nucl. Part. Sci.* **36**, 683 (1986).
 [58] K. Kumar, *Phys. Rev. Lett.* **28**, 249 (1972).
 [59] J. Srebrny and D. Cline, *Int. J. Mod. Phys.* **E20**, 422 (2011).
 [60] N. Bree *et al.*, *Phys. Rev. Lett.* **112**, 162701 (2014).
 [61] E. Clément *et al.*, *Phys. Rev. Lett.* **116**, 022701 (2016).
 [62] K. Wrzosek-Lipska *et al.*, *Phys. Rev.* **C86** 064305 (2012).
 [63] J. Srebrny *et al.*, *Nucl. Phys.* **A 766**, 25, (2006).
 [64] C. Ellegaard *et al.*, *Phys. Lett.* **40B** 641 (1972).
 [65] A. Jamshidi and W.P. Alford, *Phys. Rev.* **C8** 1782 (1973).